Supplementary information

Ordered Growth of Hexagonal and Monoclinic Phase of $MoTe_2$ on a Sapphire Substrate

Raman spectroscopy

A confocal Raman microscope (Alpha 300R, Witec, Germany) with an excitation wavelength of 532 nm was used for Raman scattering measurements. All Raman spectra were collected at room temperature using a 50x objective coupled to a 100 µm optical fibre as a confocal pinhole.

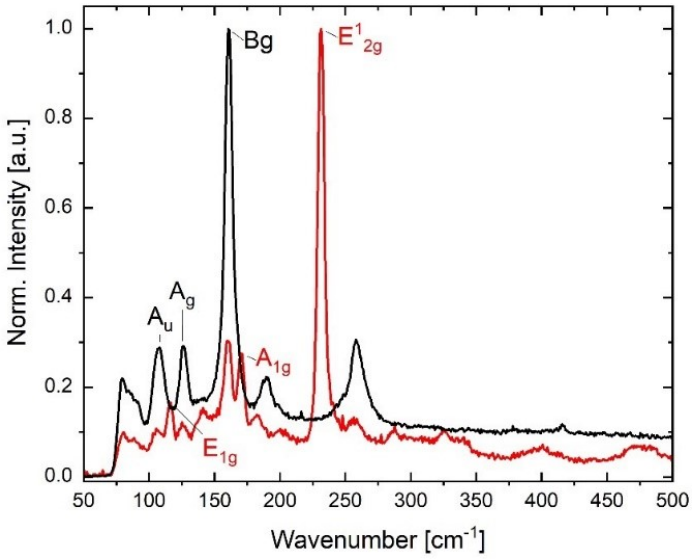

Fig. S1 Normalised Raman spectra of 2H-$MoTe_2$ (red) and 1T-$MoTe_2$ (black).

2H-MoTe has a hexagonal crystal structure and belongs to space group P63/mmc. Layers are formed by covalently bonded Te–Mo–Te atomic planes stacked along the crystallographic c-axis by weak van der Waals interactions. Each Mo atom has six neighbouring Te atoms forming trigonal prisms, slightly elongated along the c-axis.

1T'-$MoTe_2$ has a monoclinic structure and belongs to space group P21/m. The layered structure of 2H-$MoTe_2$ is maintained in 1T'-$MoTe_2$, except that Te atoms octahedrally coordinate the metal atoms. The Raman spectrum of 1T'-$MoTe_2$ reveals three bands centred at 107, 126, and 160 cm^{-1}, which are assigned to A_u, Ag, and B_g modes, respectively. The Raman spectrum of 2H-$MoTe_2$

reveals three bands centred at 117, 171, and 231.5 cm^{-1}, assigned to E_{1g}, $A_{1g,}$ and E^1_{2g} modes, respectively.

The hexagonal sample is not entirely phase-pure, as lines of the monoclinic phase are also observed in the hexagonal sample as weak features. On the other hand, the Raman lines of the monoclinic phase are much stronger than those of the hexagonal phase.[1] In addition, we did not observe any lines of the monoclinic phase in the X-ray diffraction record of the hexagonal sample. Therefore, we assume that the monoclinic phase is minor and occupies only a small volume in the hexagonal sample.

Scanning electron microscopy

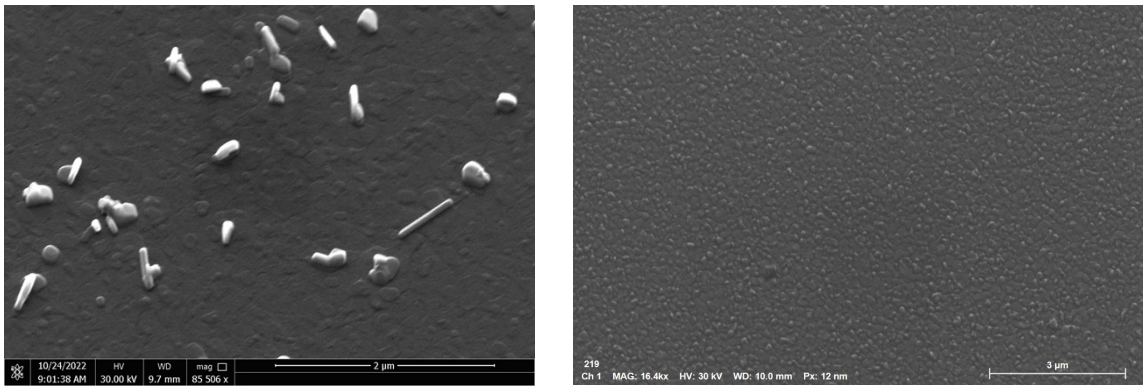

Fig. S2 SEM images of (a) 2H-$MoTe_2$ and (b) 1T-$MoTe_2$ layers.

Fig. S2 shows SEM images of the hexagonal and monoclinic layers. Both layers are made of nanocrystals with lateral sizes up to a few hundred nanometers. The surface of the hexagonal sample is relatively smooth; the protrusions are probably caused by excess tellurium, which oxidises in the air after removing the sample from the process chamber. The surface of the monoclinic sample is less smooth, with more considerable height differences between individual grains.

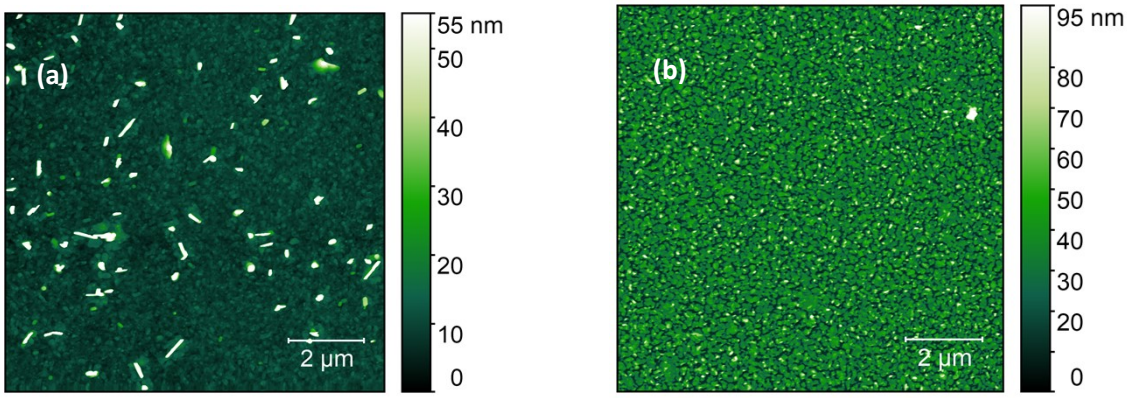

Fig. S3 AFM images of (a) 2H-$MoTe_2$ and (b) 1T´-$MoTe_2$ layers.

Atomic force microscopy

The AFM images provide similar pictures of the samples´ surface as the SEM ones shown in Fig.S2. The height of the columnar protrusions on the hexagonal sample is approximately 10 - 40 nm. The size of the crystal grains is up to 150 – 200 nm. The mean roughness of the layer is 4.5 nm (in the areas outside of the protrusions).

A closer inspection of the monoclinic sample reveals that the layer is not fully compact, with small voids between the individual island-like crystallites. The size of the crystallites is from a few tens to ~ 200 nm, and they might be as high as ~ 80 nm.

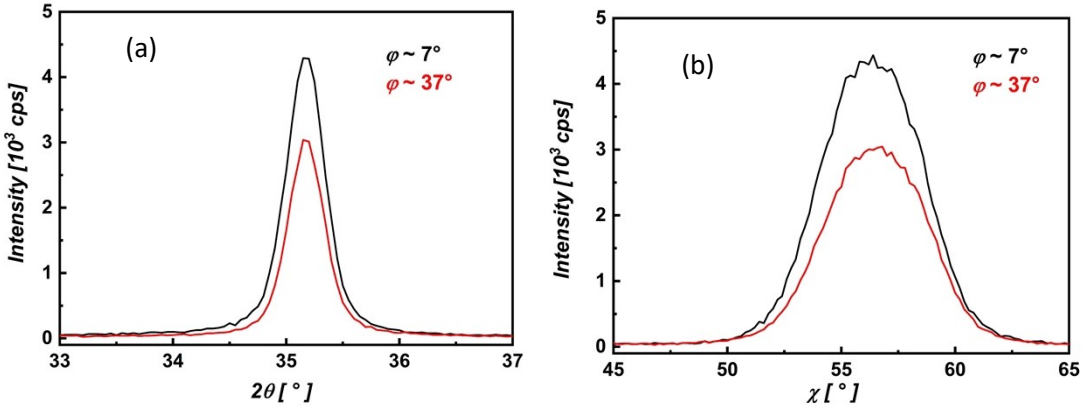

Fig. S4 (a) $2\theta/\theta$ scans across the maxima of φ-scans at ~7° (black curve) and ~37° (red curve) for the hexagonal phase. The angle χ was set to the value of 56.8°. The position of both maxima corresponds to an interplanar distance of 0.255 nm for the $10\bar{1}3$ lattice plane of hexagonal $MoTe_2$.
(b) χ-scans across the maxima of φ-scans at ~7° (black curve) and ~37° (red curve). The angle 2θ was set to the value of 35.16°. The position of both maxima corresponds to an inclination angle of 56.8° of the $10\bar{1}3$ lattice plane with respect to the c axis of hexagonal $MoTe_2$.

Hexagonal $MoTe_2$

The selections of GIWAXS patterns for hexagonal $MoTe_2$

The zooms of hexagonal $MoTe_2$ GIWAXS patterns showing 10-13 diffractions are depicted in Fig. S5 for selected angles φ. The zooms for angles of 16°, 76°, 136°, 196°, 256°, and 316° were selected, corresponding to the narrow peaks shown in Fig. 2 in the main text.

The zooms for φ angles of 47°, 107°, 165°, 228°, 287°, and 345° correspond to the broad φ scan peaks in the same figure. Fig. S4 shows non-homogenous intensity distribution in 10-13 diffraction spots for each φ angle. If two GIWAXS zoom images for φ angles mutually shifted by 180° are compared, the intensity distributions along the $\boldsymbol{q}$ vector are flipped. The uneven intensity distribution is likely due to the non-homogeneous distribution of strain along the sample length, as discussed in the main text.

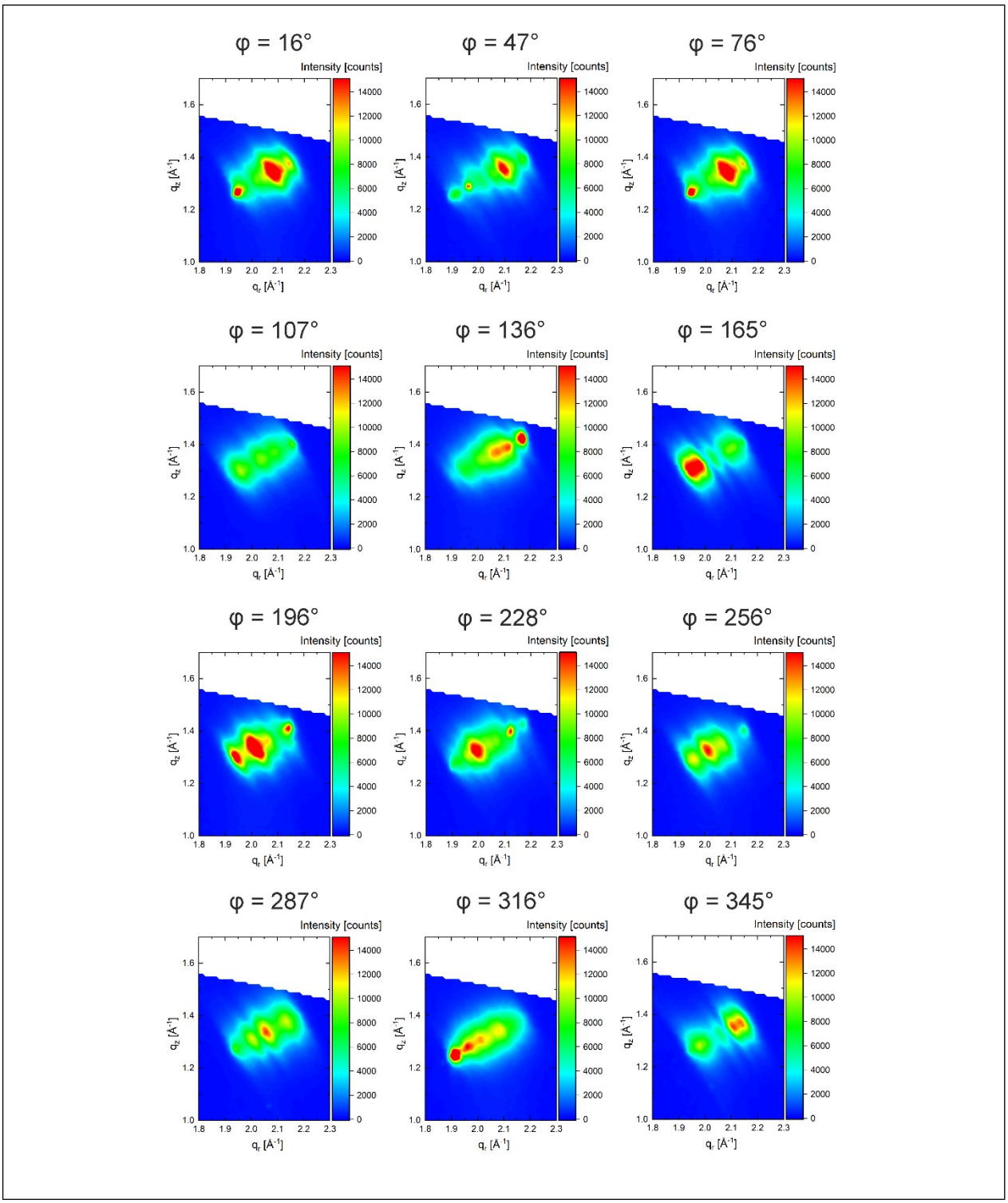

Fig. S5 The zooms of 10-13 diffraction spots measured by GIWAXS for specific φ angles.

The intensity variations in 10-10, 10-11, and 10-12 diffraction spots for various φ angles are depicted in Fig. S6. For these diffractions, we also observe non-homogeneous intensity distributions for different φ angles, similar to the 10-13 diffraction spots shown above.

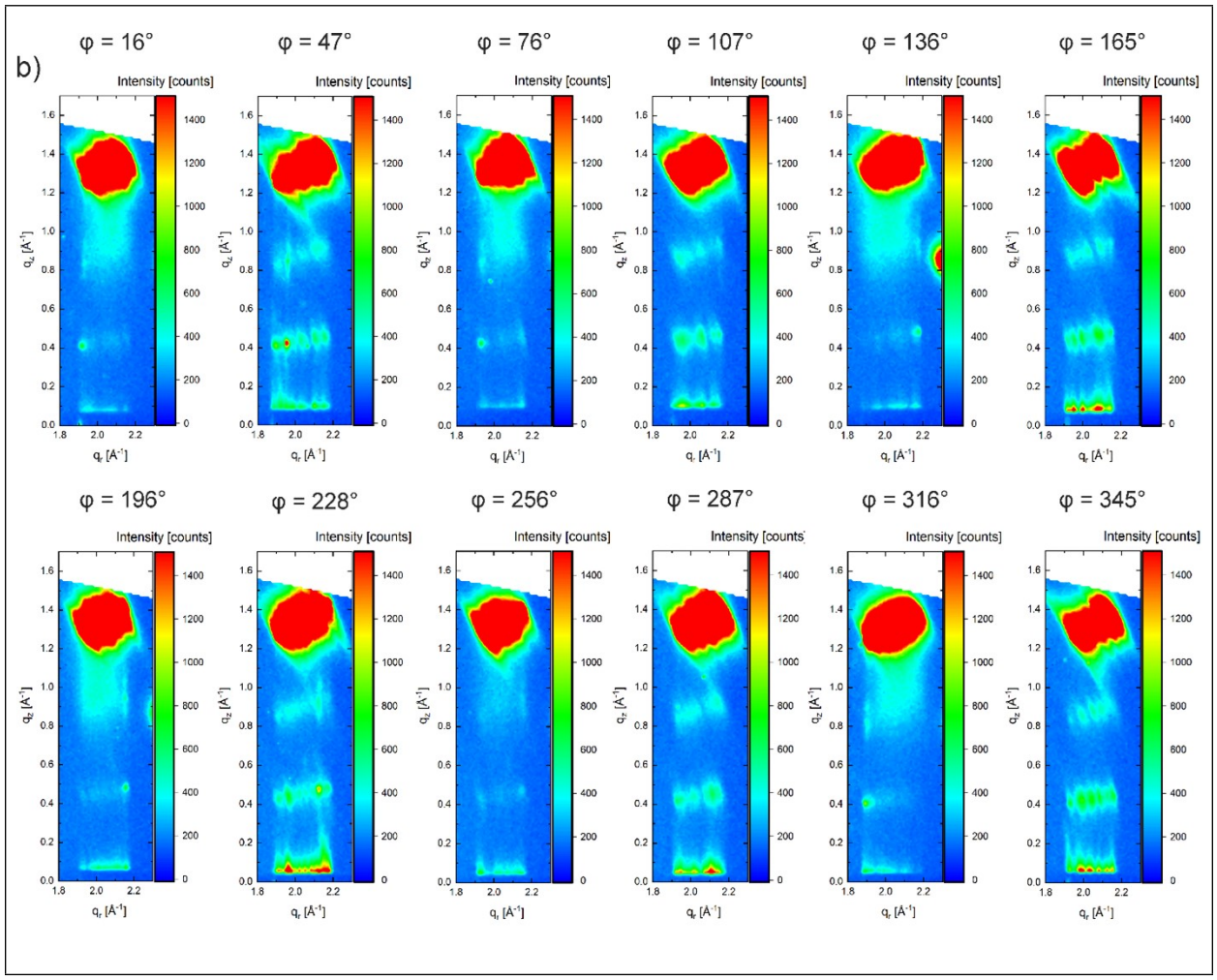

Fig. S6. The depicted lateral diffraction spots of hexagonal $MoTe_2$ (10-10, 10-11, 10-12, from bottom to top, and 10-13) for specific φ angles.

The angle between 0002 and 10-13 diffraction vectors is 58.9°. This angle corresponds to the χ angle between normal to the sample surface and the 10-13 diffraction vector. The *q*-maps were integrated between χ angles of 53°and 60°. The evolution of *q*-maps as a function of azimuthal angle φ is depicted in the colourmap in Fig. S7. Figure S8 visualises the cuts along the intensity distribution for the hexagonal $MoTe_2$ thin film.

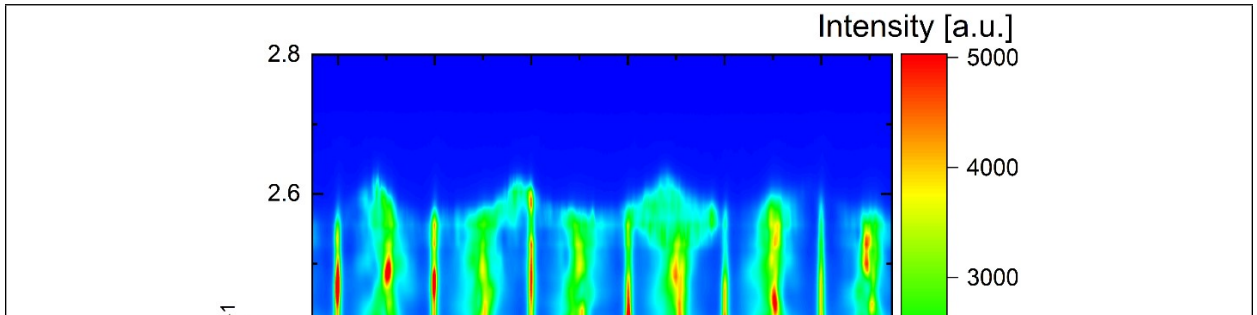

Fig. S7. The evolution of q-maps through 10-13 diffraction spot, as a function of φ angle.

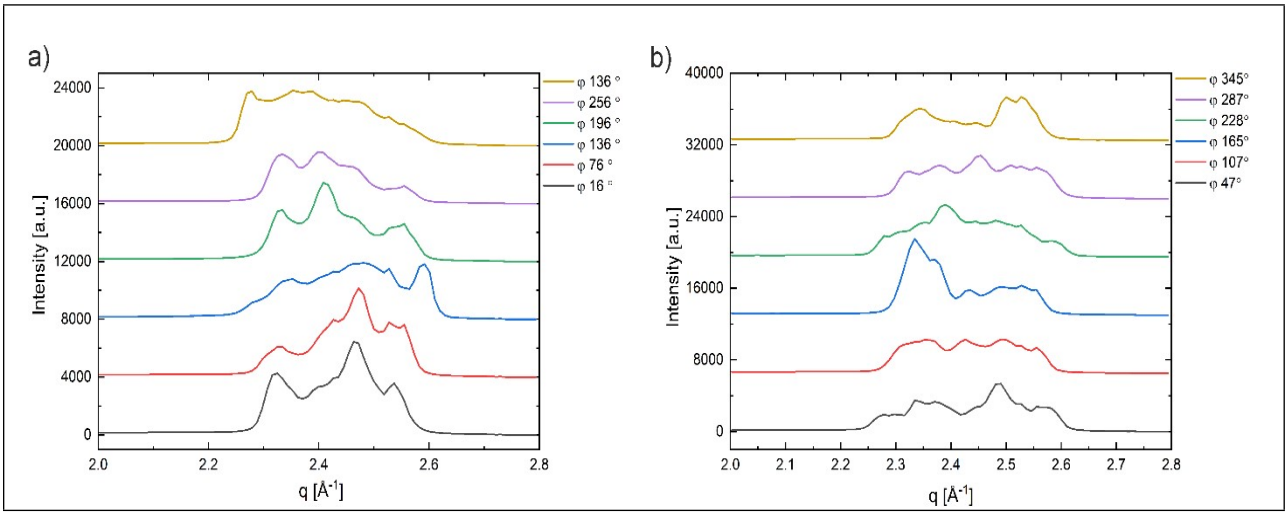

Fig. S8. The intensity evolution of the q-cuts through 10-13 diffraction spots for (a) narrow and (b) broad φ scan peaks in Fig. S7.

Monoclinic $MoTe_2$

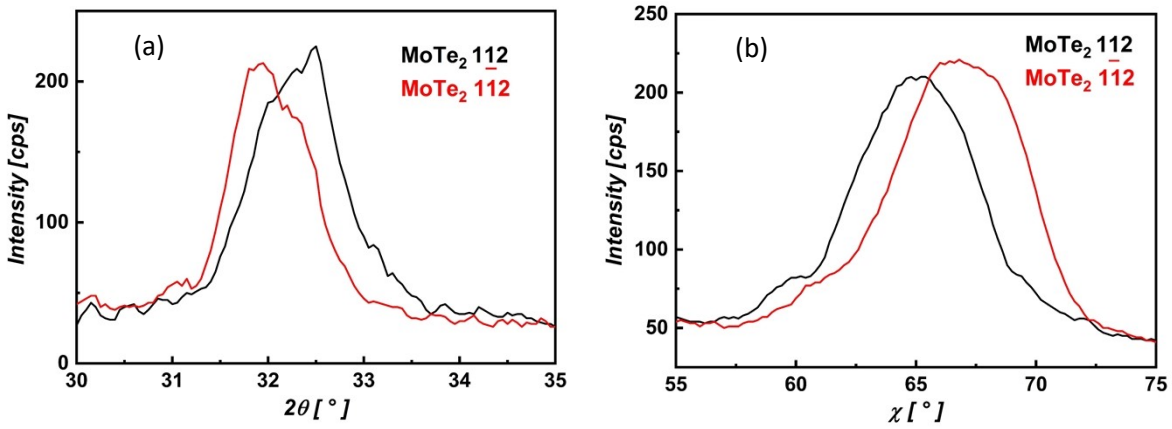

Fig. S9 (a) $2\theta/\theta$ scans across the first maximum of φ-scans at ~15°. The inclination angle χ was set to 64.7° (black curve) and 67.8° (red curve), respectively. (b) χ-scans across the first maximum of φ-scans at ~15°. The angle 2θ was set to 32.48° (black curve) and 31.93° (red curve), respectively. The position of maxima observed at the angles of 64.7° and 67.8° correspond to the inclination of $11\bar{2}$ and $\bar{1}12$ lattice planes, respectively, to the sample surface normal.

The selections of GIWAXS patterns for monoclinic $MoTe_2$

The parts of GIWAXS patterns of monoclinic $MoTe_2$ showing -112 and 112 diffractions for selected φ angles are depicted in Fig.S10. The GIWAXS patterns for φ angles of 14°, 71°, 134°, 194°, 253°, and 314° correspond to the more intense φ scan peaks in Fig.6a and 6b in the main text. The GIWAXS patterns for φ angles of 43°, 104°, 163°, 223°, 284°, and 343° correspond to the less intense φ scan peaks in the same figure. The intensity distribution within the diffraction spot is much more uniform compared to the hexagonal phase.

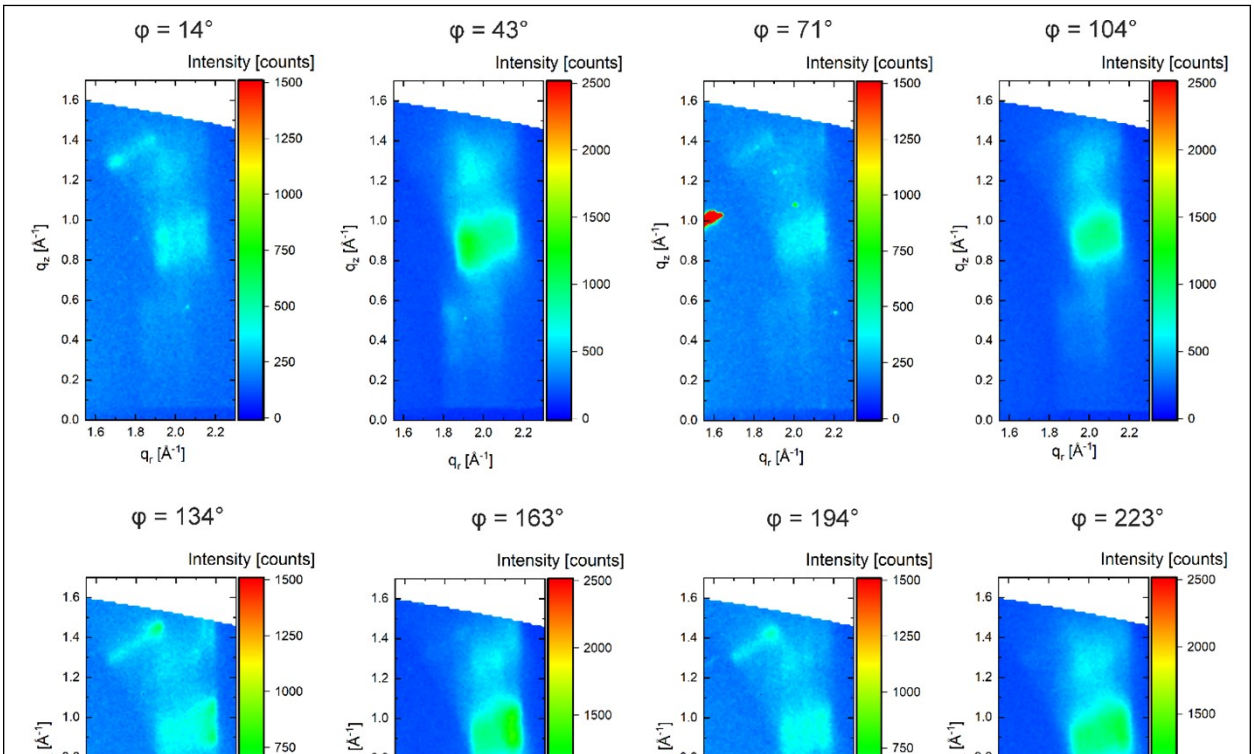

Fig. S10 The depicted lateral diffraction spots of monoclinic $MoTe_2$ (-112 and 112) for specific φ angles.

The angle between 002 and -112 diffraction vectors is 67.8°, and the angle between 002 and 112 diffraction vectors is 64.6°. Therefore, the q-cuts were integrated between χ angles of 62°and 70°. The evolution of q-cuts as a function of azimuthal angle φ is depicted in the colourmap in Fig. S11, and the corresponding q-cuts are shown in Fig. S12.

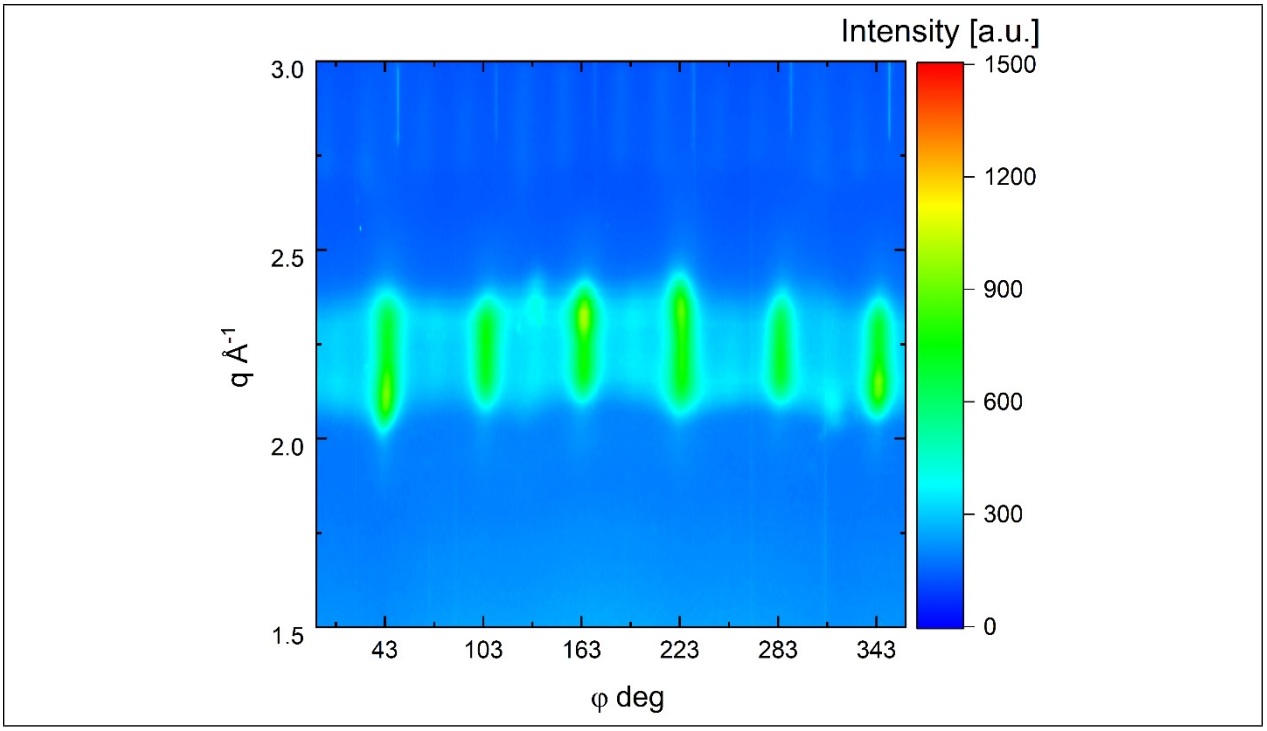

Fig. S11 The evolution of q-maps through -112 and 112 diffraction spots for different φ angles.

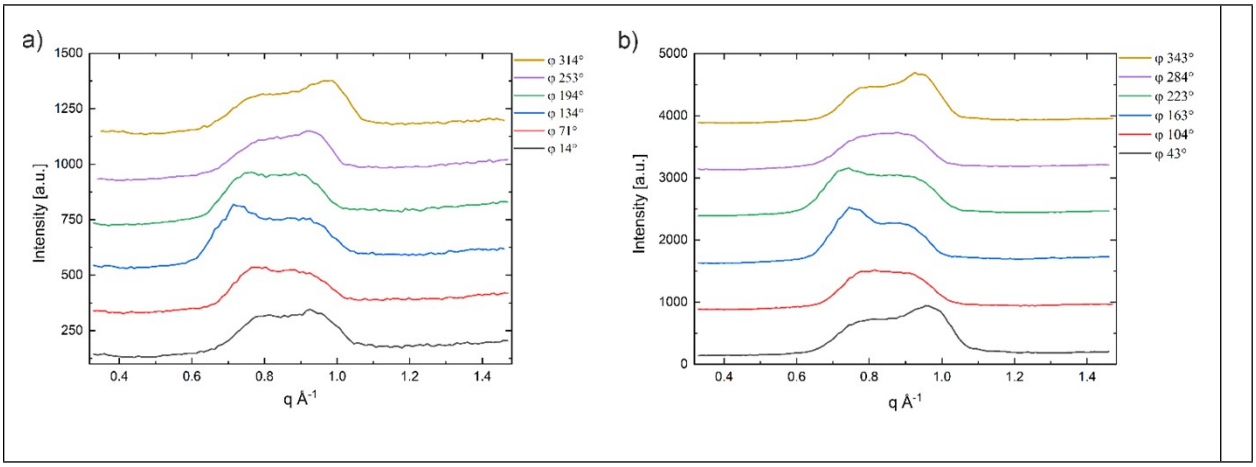

Fig. S12 The evolution of the intensity q-cuts through -112 and 112 diffraction spots for (a) minor and (b) dominant φ scan peaks in Fig.6b of the main text.

References

1.T. A. Empante, Y. Zhou, V. Klee, A. E. Nguyen, I.-H. Lu, M. D. Valentin, S. A. Naghibi Alvillar, E. Preciado, A. J. Berges, C. S. Merida, M. Gomez, S. Bobek, M. Isarraraz, E. J. Reed and L. Bartels, *ACS Nano*, 2017, **11**, 900–905.